

Novel Spectrum Sensing Methods for OFDM Systems Using Deep Learning Networks

Qingqing Cheng, *Student Member, IEEE*, Zhenguo Shi,
Diep N. Nguyen, *Member, IEEE*, and Eryk Dutkiewicz, *Senior Member, IEEE*

Abstract—Spectrum sensing of orthogonal frequency division multiplexing (OFDM) signals has been widely regarded as a potential solution to address spectrum shortages in cognitive radio networks. Despite the effectiveness of improving spectrum utilization, conventional OFDM sensing methods suffer from noise uncertainty, timing delay and carrier frequency offset (CFO), which can significantly degrade sensing performance. To overcome those problems, we propose two novel OFDM sensing methods drawing support from deep learning networks. Specifically, we propose a stacked autoencoder based spectrum sensing method (SAE-SS), in which a stacked autoencoder network is designed to detect the activity states of PUs by automatically extracting the inherent features from the original received OFDM signals. The proposed SAE-SS is more robust to noise uncertainty, timing delay and CFO than the conventional OFDM sensing methods. Moreover, SAE-SS does not require any prior information of PU’s signals which are essential for the conventional feature-based OFDM sensing methods. Additionally, to further improve the sensing performance of SAE-SS under low SNR conditions, we propose a stacked autoencoder based spectrum sensing method with time-frequency domain signals (SAE-TF). SAE-TF can achieve a higher sensing accuracy than SAE-SS at the expense of complexity. Extensive simulation results show that both SAE-SS and SAE-TF can achieve much better sensing accuracy, compared with state of the art approaches, suffering from noise uncertainty, timing delay and CFO, respectively.

Index Terms—Cognitive radio networks, OFDM, deep learning, SAE.

I. INTRODUCTION

THE dynamic spectrum access (DSA) has received its recognition as a potential solution to solve the spectrum shortage problem in the cognitive radio networks (CRNs) [1]. In DSA, secondary users (SUs) are allowed to exploit the under-utilized spectrum of primary users (PUs) without causing any harmful interference to those PUs. To that end, SUs is required to detect the activity states of PUs (e.g., absence or presence) reliably before utilizing PU’s spectrum bands, which is the critical task of spectrum sensing techniques [2]. In the context of sensing techniques, the spectrum sensing of orthogonal frequency division multiplexing (OFDM) signals has been regarded as a promising candidate and attracts great attention [3].

The efforts of OFDM sensing methods in the literature can be categorized into two main types: non-cooperative OFDM sensing methods and cooperative OFDM sensing methods [4]. For the non-cooperative OFDM sensing, a single SU can decide PU’s activity states by applying sensing methods. For the cooperative OFDM sensing methods, each SU makes a local decision and all those decisions are reported to a fusion

center to achieve a final decision based on some fusion rules [5]. In this work, we focus on the non-cooperative OFDM sensing methods.

The energy detection (ED) is one of the simplest and most popular sensing methods, which senses PU’s activity states based on the received signals’ energy [6], [7]. However, it is vulnerable to the noise uncertainty, and the uncertainty of noise variance would cause significant degradation on sensing performance, which prohibits its promotion in practice [8], [9]. Matched filtering (MF) is superior to ED regarding the robustness to noise uncertainty, while it is sensitive to timing delay [10].

The feature-based detections are proposed to detect the presence of the PU’s signals by leveraging special structure features of OFDM signals (such as pilot tones (PT) [11]–[13] and cyclic prefix (CP) features [14]–[16]). For instance, authors in [12] propose a PT-based method to sense the attendance of PUs by utilizing the cross-correlation among the time-domain symbols. In [13], the authors present a pilot-assisted spectrum sensing method by exploiting either the first-order or the second-order statistical difference between the pilot and payload subcarriers. Although these PT-based OFDM sensing methods can sense the attendance of PUs’ signals reliably, they have high computational complexities and are vulnerable to carrier frequency offset (CFO) [17]. For the CP-based sensing methods, [15] and [16] present CP-based methods drawing support from the CP’s autocorrelation property and cyclostationarity property, respectively. However, the sensing performance is compromised with the length of CP and the synchronization errors/timing delay [18]. In addition, the feature-based sensing methods require full or partial prior knowledge of PU’s signals (e.g., PU’s transmitting power, the CP or PT structure of PU signals) and/or noise power to complete the sensing task, which is unavailable in some practical applications [19].

Machine learning (ML) is another promising technique for spectrum sensing, which has been widely investigated in many fields such as object detection [20], [21], speech recognition [22], [23], channel estimation [24], and pattern recognition [25], [26]. Most ML sensing methods regard the spectrum sensing processing as the pattern recognition [27], as shown in Fig. 1. Specifically, the pattern recognition involves the steps of the feature extraction and the classification [28], [29]. For the typical OFDM sensing methods, they also include two steps: first, calculate the test statistic of the received signals; second, compare the test statistic with the corresponding thresholds to detect PU’s activity states. Consequently, the

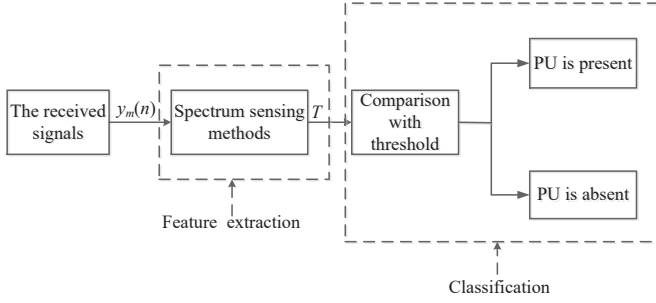


Fig. 1. Relationship between spectrum sensing and pattern recognition

first and second stages in OFDM sensing process are regarded as the feature extraction and the classification in pattern recognition, respectively. In other words, ML based sensing methods sense the PU's activity states using the features obtained from the feature extraction processing. For example, the authors in [30] present an artificial neural network based sensing algorithm, which uses the energy feature as the input feature. In [31] and [32], authors apply both the energy and cyclostationary features as the input feature and propose spectrum sensing methods based on artificial neural networks, respectively. Although those ML based sensing methods mentioned above can improve the sensing accuracy, they still suffer from some drawbacks. First, since the methods above use the energy features or cyclostationary features as input features, their sensing performance is compromised with noise uncertainty, timing delay, CFO, etc. Second, extracting specific features from the original received signals can only achieve the partial information, which will inevitably lose some useful information and reduce the sensing accuracy.

For the above, it is very much desirable to present a novel spectrum sensing method to overcome all the limitations of the methods above. To that end, we propose two OFDM sensing methods by leveraging deep learning networks [33], [34]. Deep learning, one of the most important candidates of ML [35], leverages deep architectures (e.g., multiple layers of nonlinear processing units) to extract and transform the inherent features from the input signals [36]. In this work, we present two sensing methods drawing support from the stacked autoencoder (SAE) [37] to detect PU's activity states by automatically extracting inherent features from the original received signals. Main contributions of this paper are summarized as follows.

- We propose the stacked autoencoder based spectrum sensing method (SAE-SS) to extract inherent features of the original received signals and detect the PU's activity states based on the extracted features.
- Compared with traditional OFDM sensing methods, the proposed SAE-SS is more robust to timing delay, noise uncertainty and CFO. Moreover, SAE-SS can sense the PUs activity states using the original received signals only without requiring any prior knowledge of PUs signals.
- Unlike the OFDM sensing methods that need algorithms to extract some features from the original received signals for sensing purpose, SAE-SS is able to automatically extract the inherent features from the original received

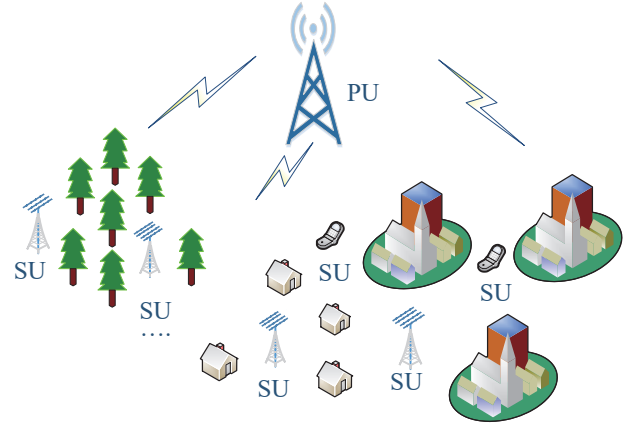


Fig. 2. OFDM based cognitive radio system

signals without any additional feature extraction algorithms.

- To further improve the sensing performance of SAE-SS under low SNR conditions, we propose a stacked autoencoder based spectrum sensing method using time-frequency domain signals (SAE-TF). SAE-TF can achieve get a better sensing accuracy by leveraging the time-frequency domain signals at the cost of higher computational complexity.
- We carry out extensive simulations to evaluate the performance of SAE-SS and SAE-TF. The simulation results show that our proposed methods are capable of achieving much better sensing accuracies than the conventional OFDM sensing methods under poor communication conditions (e.g., timing delay, noise uncertainty and CFO).

The rest of this paper is organized below. Section II is a description of the system model and problem formulation. Section III describes the details of SAE-SS. Section IV presents the details of SAE-TF. Experimental results are shown in Section V, followed by the conclusion of this paper in Section VI.

II. SYSTEM MODEL AND PROBLEM FORMULATION

A. System Model

A typical OFDM-based cognitive radio system applied in this work is shown in Fig. 2. Each SU opportunistically utilizes the PU's licensed spectrum bands by detecting that PU's activity states. Let $y_m(n)$ denotes the received discrete time signal at the SU receptor, where $m = 0, \dots, M-1$, and M is the total number of received OFDM blocks. $n = 0, \dots, N_c + N_d - 1$, N_c is the length of cyclic prefix and N_d is the data block size. Then $y_m(n)$ is

$$H_0 : y_m(n) = w_m(n),$$

$$H_1 : y_m(n) = e^{-j \frac{2\pi f_q(n-\delta)}{N_d}} \sum_{l=0}^{L_p-1} h_{ls} s_m(n-\delta-l) + w_m(n), \quad (1)$$

where H_0 and H_1 represent the absence and the presence of PU, respectively. $w_m(n)$ means the complex additive white Gaussian noise (AWGN) with zero-mean and variance σ_w^2

(i.e., $w_n(m) \sim CN(0, \sigma_w^2)$). $s_m(n)$ denotes the transmitted OFDM signals by PU transmitter. f_q is the normalized carrier frequency offset. δ stands for the timing delay. h_l represents the channel gain of the l th channel and its value does not change during the sensing stage. L_p means the total number of multi-path components between the PU and the SU. Without loss of generality, $w_m(n)$, $s_m(n)$ and h_l are assumed to be independent with each other. According to the central limit theorem, when the length of received signals is sufficiently large, $s_m(n)$ approximately obeys the complex Gaussian distribution, and its mean and variance are zero and σ_s^2 , respectively. In that case, SNR of $y_m(n)$ under H_1 can be represented as $\text{SNR} = \sigma_s^2 \sum_{l=0}^{L-1} |h_l|^2 / \sigma_w^2$.

B. Problem Formulation

For typical OFDM sensing methods, take the ED as an example, its test statistic T_{en} is

$$T_{en} = \frac{1}{M(N_c + N_d)} \sum_{m=0}^{M-1} \sum_{n=0}^{N_c + N_d - 1} |y_m(n)|^2. \quad (2)$$

The probability of false alarm (PFA) and probability of miss detection (PM) for energy detection are

$$\begin{aligned} \text{PFA}_{en} &= \Pr(T_{en} > \lambda | H_0), \\ \text{PM}_{en} &= 1 - \Pr(T_{en} > \lambda | H_1), \end{aligned} \quad (3)$$

where λ is the sensing threshold based on the estimated noise variance ($\tilde{\sigma}_w^2$). According to equation (2) and (3), ED only utilizes the received signals to detect the presence of PU without requiring any prior knowledge of PU signals. However, it is vulnerable to the noise uncertainty, and a small estimated error in the noise power would significantly deteriorate its sensing performance, especially under low SNR conditions [8].

For feature-based detections, such as CP-based or PT-based sensing methods, their test statistics are

$$\begin{aligned} T_{cp} &= \sum_{i=0}^{N_c + N_d - 1} \frac{\mu_{1,i}}{\sigma_{0,i}^2} \Re(R_i), \\ R_i &= \sum_{m=0}^{M-1} \sum_{j=0}^{N_c - 1} y_m^*(i+j) y_m(i+j+N_d), \end{aligned} \quad (4)$$

$$T_{pt} = \sum_{N_v}^{N_p - 1} \sum_{i=0}^{N_v} y_m^*(i) y_k(i), \quad (5)$$

where $\mu_{1,i}$ stands for the mean of $R_i | H_1$. $\sigma_{0,i}^2$ is the variance of $R_i | H_0$. $\Re(\cdot)$ means the real part, and $(\cdot)^*$ represents the complex conjugate operation. N_v is the number of block pairs (m, k) with the same PT arrangement. N_p denotes the length of PT.

Although CP-based and PT-based detections are able to overcome the noise uncertainty, they require some prior knowledge, such as the PU's transmitting power, CP (N_c) or PT (N_p and N_v) structure of PU signals, which are usually not available in the practical environment. Moreover, the feature-based detections are sensitive to timing delay and CFO, and

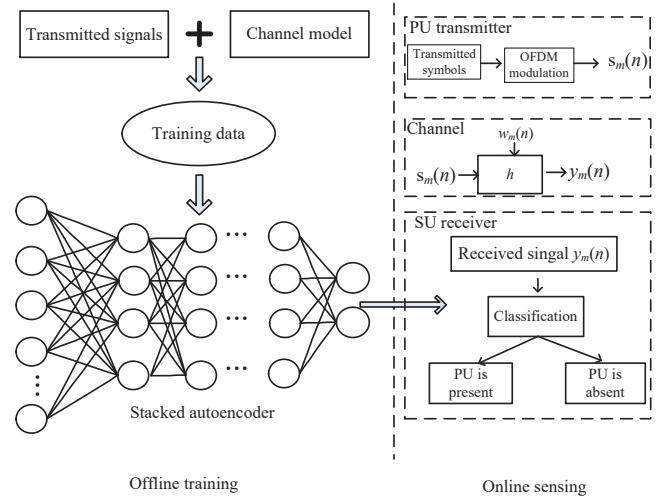


Fig. 3. Architecture of the OFDM system with SAE-SS

even a small mismatch between the received and transmitted signals in the time domain or frequency domain would cause significant degradation of sensing accuracy.

To overcome the drawbacks associated with traditional OFDM sensing methods, we propose a novel spectrum sensing methods based on Stacked SAE network.

III. PROPOSED STACKED AUTOENCODER BASED SPECTRUM SENSING METHOD

In this section, we propose SAE-SS that is robust to timing delay, noise uncertainty and CFO. The architecture of the OFDM system with SAE-SS is shown in Fig. 3. The inherent features of received OFDM signals are extracted from the SAE network during the offline training stage. Then those extracted features are used to sense PU's activity states during the online sensing stage. The key steps of SAE-SS can be summarized as: pretraining, fine-tuning of SAE and classification (e.g., online spectrum sensing stage) [37].

A. Pretraining of Stacked Autoencoder

The pretraining SAE aims to learn the inherent features of received signals through two stages: first, divide the SAE network into independent Autoencoders (AEs) and train these AEs one by one. AE is a three-layer network includes input layer, hidden layer and reconstruction layer, which is illustrated in Fig. 4(a); second, stack the input and hidden layers of all the trained AEs together layer by layer, as shown in Fig. 4(b).

In this work, the number of input units for the first AE is the integral multiple of OFDM blocks. Moreover, since AE is only suitable for the non-complex numbers, we divide the input signals into the real and imaginary parts, respectively. Therefore, the signals in equation (1) is

$$\begin{aligned} y_i := \{ & \Re(y_i(0)), \Im(y_i(0)), \Re(y_i(1)), \Im(y_i(1)), \dots, \\ & \Re(y_i(N_c + N_d - 1)), \Im(y_i(N_c + N_d - 1)) \}, \end{aligned} \quad (6)$$

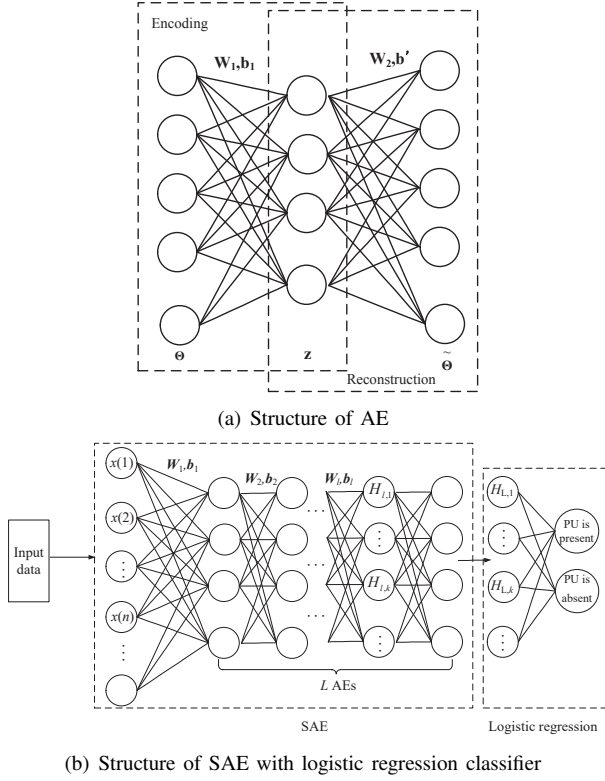


Fig. 4. The structure of spectrum sensing based on traditional neural networks

where $\Im(\cdot)$ means the imaginary part. Thus the input vector of SAE-SS network \mathbf{x} can be expressed as

$$\mathbf{x} := \{\mathbf{y}_0, \mathbf{y}_1, \dots, \mathbf{y}_{M-1}\}^T, \quad (7)$$

where the length of \mathbf{x} is equal to $N_{input} = 2M(N_c + N_d)$. Then the input signals \mathbf{x} are used to train AEs.

For each AE, its input data is the output data of the previous AE, and its output will act as the input data of the next AE. Take the l th AE as an example, let $H_{l,p}^{in}$, $H_{l,k}$ and $H_{l,q}^{out}$ stand for the p th input unit, the k th hidden unit and the q th output unit, respectively. The relationships among them are

$$H_{l,k} = f\left(\sum_{p=1}^{N_{l-1}} W_{l,p,k} H_{l,p}^{in} + b_{l,k}\right), \quad (8)$$

$$\begin{aligned} H_{l,q}^{out} &= f\left(\sum_{k=1}^{N_l} W'_{l,k,q} H_{l,k} + b'_{l,q}\right) \\ &= f\left(\sum_{k=1}^{N_l} W'_{l,k,q} f\left(\sum_{p=1}^{N_{l-1}} W_{l,p,k} H_{l,p}^{in} + b_{l,k}\right) + b'_{l,q}\right) \end{aligned} \quad (9)$$

where N_l is the number of units in the l th AE. N_{l-1} is the number of units in the $(l-1)$ th AE. $W_{l,p,k}$ stands for the weight between the p th input unit and the k th hidden unit of the l th AE. $W'_{l,k,q}$ denotes the weight between the k th hidden unit and the q th output unit of the l th AE. $W_{l,p,k} = W'_{l,k,q}$. $b_{l,k}$ and $b'_{l,q}$ are the bias of the k th input unit and q th output unit of the l th AE, respectively.

When $l = 1$, then $\mathbf{H}_1^{in} = \mathbf{x}$, which is

$$\mathbf{H}_1^{in} := \{H_{11}^{in}, H_{12}^{in}, \dots, H_{1N_0}^{in}\}^T, \quad (10)$$

where N_0 is the number of input units in the first AE, $N_0 = N_{input} = 2M(N_c + N_d)$.

In this paper, the sigmoid function is adopted as the activation function, which is expressed as

$$f(H_{l,p}^{in}) = \frac{1}{1 + e^{-H_{l,p}^{in}}}. \quad (11)$$

The aim of training the l th AE is to minimize the error between $H_{l,p}^{in}$ and $H_{l,p}^{out}$ by continuously updating the values of $W_{l,p,k}$, $b_{l,k}$ and $b'_{l,q}$. The most typical error function to measure the difference between $H_{l,p}^{in}$ and $H_{l,p}^{out}$ is mean square error:

$$\chi = \sum_{p=1}^{N_{l-1}} \|H_{l,p}^{in} - H_{l,p}^{out}\|^2. \quad (12)$$

However, this method is time-consuming for training, thus we select the cross-entropy to speed up the training process, which is

$$\chi = \sum_{p=1}^{N_{l-1}} [H_{l,p}^{in} \log(H_{l,p}^{out}) + (1 - H_{l,p}^{in}) \log(1 - H_{l,p}^{out})]. \quad (13)$$

Let $\Omega = \{W_{l,p,k}, b_{l,k}, b'_{l,q}\}$, then the object function is

$$\Omega = \arg \min_{\Omega} \chi(H_l^{in}, H_l^{out}). \quad (14)$$

Moreover, we adopt the gradient descent method [38] to achieve the optimal Ω , and the rules of updating Ω are

$$W_{l,p,k}(n+1) \leftarrow W_{l,p,k}(n) - \kappa \frac{\partial \chi(H_l^{in}, H_l^{out})}{\partial W_{l,p,k}}, \quad (15)$$

$$b_{l,k}(n+1) \leftarrow b_{l,k}(n) - \kappa \frac{\partial \chi(H_l^{in}, H_l^{out})}{\partial b_{l,k}}, \quad (16)$$

$$b'_{l,q}(n+1) \leftarrow b'_{l,q}(n) - \kappa \frac{\partial \chi(H_l^{in}, H_l^{out})}{\partial b'_{l,q}}, \quad (17)$$

where $W_{l,p,k}(n)$, $b_{l,k}(n)$ and $b'_{l,q}(n)$ denote the weight and bias of n th training. κ is the learning rate.

Upon training all the AEs based on the above rules, the trained SAE is created by stacking the input and hidden layers of trained AEs together layer by layer. The output of SAE's pre-training, which is also the hidden units of L th AE, can be written as

$$\mathbf{H}_L := \{H_{L1}, H_{L2}, \dots, H_{LN_L}\}^T. \quad (18)$$

\mathbf{H}_L in equation (18) contains the inherent features of the received signals and will be used to sense the PU's activity states.

B. Fine-Tuning and Classification

The pretraining processes of SAE can be treated as extracting the PU's unsupervised features. Thus, the trained SAE needs to be fine-tuned to leverage the SAE's property for

the spectrum sensing. In this paper, we select the logistic regression classifier to fine-tune the SAE network, as shown in Fig. 4(b).

The logistic regression classifier can be regarded as a neural network with a single layer, and the activation of output layer is the softmax function. The input of the logistic regression classifier is \mathbf{H}_L , which is the output of the pretraining SAE. U which is the output of logistic regression classifier, can be seen as a set of conditional probabilities of \mathbf{H}_L , \mathbf{W}_R and \mathbf{b}_R . \mathbf{W}_R and \mathbf{b}_R are weights and biases of the logistic regression layer. Notably, SAE is used to sense the PU's activity states (e.g., absence or presence), which can be seen as a binary classification. Let $\tau = 1$ and $\tau = 0$ stand for the presence and the absence of PU, respectively. Then the conditional probability of U is

$$P(U=\tau|\mathbf{H}_L, \mathbf{W}_R, \mathbf{b}_R) = \frac{e^{\mathbf{W}_{R,\tau}\mathbf{H}_L + \mathbf{b}_{R,\tau}}}{\sum_{i=0}^1 e^{\mathbf{W}_{R,i}\mathbf{H}_L + \mathbf{b}_{R,i}}}. \quad (19)$$

We apply the backpropagation method to train the logistic regression classifier, and the whole SAE network is also fine-tuned at the same time.

Upon pretraining and fine-tuning the SAE network in the offline phase, SAE-SS is able to detect the PU's activity states based on the received signals only. Compared with the feature-based OFDM spectrum sensing methods (e.g., CP-based and PT-based), the inputs of SAE-SS are original received signals without requiring any arithmetical operations such as calculating the energy or the correlation values. Consequently, the overheads of SAE-SS considering both offline training and online sensing are reduced significantly. Moreover, the proposed SAE-SS can complete the sensing task without any prior knowledge of the PU's information, which is more suitable for the practical environment. The procedure of SAE-SS is summarized in Summary 1.

IV. PROPOSED STACKED AUTOENCODER BASED SPECTRUM SENSING METHOD WITH TIME-FREQUENCY DOMAIN SIGNALS

As aforementioned, the proposed SAE-SS can achieve a good sensing performance with the original received signals and does not require any additional feature extraction algorithms, which can reduce the complexity. However, its sensing accuracy would degrade under low SNR conditions. To address that problem, we present a Stacked Autoencoder Based Spectrum Sensing Method with time-frequency domain signals (SAE-TF). SAE-TF is able to provide both time domain and frequency domain signals, which is beneficial for SAE to extract more inherent features for the spectrum sensing purpose. The framework of SAE-TF is shown in Fig. 5.

The first step of SAE-TF is to transfer the original received signals from the time domain to the frequency domain by Fast Fourier transform (FFT), by

$$\mathbf{Y} = \text{FFT}(\mathbf{y}), \quad (20)$$

where $\text{FFT}(\cdot)$ stands for the FFT operation. Then \mathbf{Y} is divided into real and imaginary parts, respectively. Under this

Summary 1: Stacked Autoencoder Based Spectrum Sensing Method (SAE-SS)

```

1: begin
2: Initialize: the length of input  $N_{input}$ , number of SAE
   layer  $L$ , the number of unit in  $l$ th layer  $N_l$ ,
   pretraining iterations  $N_{pr}$ , pre-training learning rate  $\kappa_p$ ,
   fine-tuning iterations  $N_f$ , fine-tuning rate  $\kappa_f$ ,
   number of classes  $C$ ;
3: Achieve  $\mathbf{x}$  based on  $\mathbf{y}$ 
4: For  $1 \leq l \leq L$ 
5:   Build an AE with  $N_v$  units of input layer and  $N_h$  unit
     of hidden layer;
6:   If  $l = 1$ 
7:      $N_v = N_{input}$ ;
8:      $N_h = N_1$ ;
9:      $\mathbf{x}$  is set as the input of AE;
10:  else
11:     $N_v = N_{l-1}$ ;
12:     $N_h = N_l$ ;
13:    the output of previous layer  $H_{l-1}$  is set as the
      input of current layer  $H_l^{in}$ ;
14:  end
15: Initialize AE, generate  $\mathbf{W}_l$ ,  $\mathbf{b}_l = \mathbf{b}'_l = 0$ 
16: For  $1 \leq t \leq N_{pr}$ 
17:   Based on (8) calculate the output of reconstruction:
      $H_{l,q}^{out} = f(\sum_{k=1}^{N_l} W'_{l,k,q} H_{l,k} + b'_{l,q})$ 
18:   Based on (13) calculate the error:
      $\chi = \sum_{p=1}^{N_{l-1}} [H_{l,p}^{in} \log(H_{l,p}^{out}) + (1 - H_{l,p}^{in}) \log(1 - H_{l,p}^{out})]$ 
19:   Based on (15)-(17) update  $\mathbf{W}_l$ ,  $\mathbf{b}_l$  and  $\mathbf{b}'_l$  with  $\kappa_p$ 
20: end
21: remove the reconstruction layer of AE
22: end
23: Initialize logistic regression layer:  $N_L$  unit of input layer,
      $C$  unit of output layer
24: For  $1 \leq t \leq N_f$ 
25:   Based on (19) calculate probability of each class
26:   Based on back propagation, update parameters of
     every layer with  $\kappa_f$ 
27: end

```

situation, the frequency domain signals are expressed as

$$\mathbf{Y}_i := \{\Re(Y_i(0)), \Im(Y_i(0)), \dots, \Re(Y_i(N_c + N_d - 1)), \Im(Y_i(N_c + N_d - 1))\}. \quad (21)$$

Thus the frequency domain input vector of SAE-SS network \mathbf{X} can be expressed as

$$\mathbf{X} := \{\mathbf{Y}_0, \mathbf{Y}_1, \dots, \mathbf{Y}_{M-1}\}^T, \quad (22)$$

where the length of \mathbf{X} is equal to $N_{input} = 2M(N_c + N_d)$.

Then the input signals, which are the linear arrangement of \mathbf{x} and \mathbf{X} , are fed into the SAE network for training, as shown in Fig. 5. After pre-training, fine-tuning of SAE and classification, which are the same with Section III, SAE-TF can better probe the activity states of the PU than SAE-SS based on the extracted inherent features. Notably, SAE-TF outperforms SAE-SS under low SNR conditions with the help of time domain and frequency domain features. However, the number of input units of SAE-TF doubles that of SAE-SS, so the training complexity is higher. The procedure of SAE-SS is summarized in Summary 2.

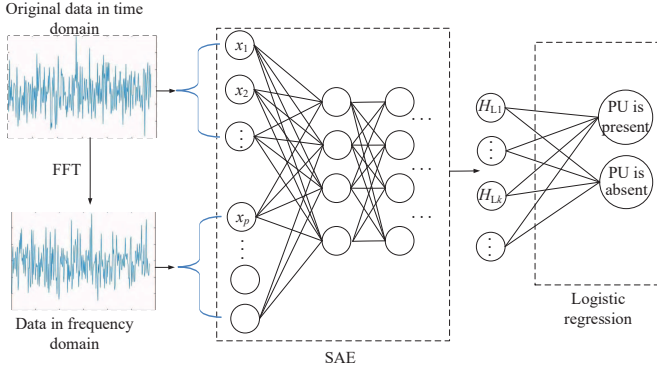


Fig. 5. Structure of proposed SAE-TF with logistic regression classifier

Summary 2: Proposed Stacked Autoencoder Based Spectrum Sensing Method with Time-Frequency Domain Signals (SAE-TF)

```

1: begin
2: Transfer the received signals  $\mathbf{y}$  using FFT and obtain  $\mathbf{Y}$ 
3: Achieve  $\mathbf{x}$  and  $\mathbf{X}$  based on  $\mathbf{y}$  and  $\mathbf{Y}$ 
4: For  $1 \leq l \leq L$ 
5:   Build an AE with  $N_v$  units of input layer and  $N_h$  units
   of hidden layer;
6:   If  $l = 1$ 
7:      $N_v = 2 * N_{input}$ ;
8:      $N_h = N_1$ ;
9:     The input signals of the first AE are the linear
   arrangement of  $\mathbf{x}$  and  $\mathbf{X}$ ;
10:  else
11:     $N_v = N_{l-1}$ ;
12:     $N_h = N_l$ ;
13:    the output of previous layer  $H_{l-1}$  is set as the
   input of current layer  $H_l^{in}$ ;
14:  end
15: Train SAE-TF with the input signals.
   Training procedures are the same to Summary 1.
16: end

```

V. SIMULATION RESULTS

In this section, we first conduct numerous simulations to analyze the performance of the proposed two methods (e.g., SAE-SS and SAE-TF) and other three conventional OFDM sensing methods (e.g., ED method in [7], PT-based sensing method [11] and CP-based sensing method in [14]). Then we provide the performance analysis of SAE-SS with different parameters. The propagation channel between PU transmitter and SU receiver is frequency selective Rayleigh fading channel. The OFDM block size of the PU signal is set to $N_d = 64$, CP length is $N_c = N_d/8$, and PT is selected as $N_p = 10$. We set the probability of false alarm $PF = 0.05$. The length of input for SAE-SS and SAE-TF are $N_{input} = 2M(N_c + N_d)$ and $N_{input} = 2 * 2M(N_c + N_d)$, respectively, and $M = 2$. The number of units in the first and the second hidden layer for both SAE-SS and SAE-TF are 100 and 50, respectively. The number of training data set contains $2 * 10^4$, which is the same as the number of testing data set. The number of interactions is 5000.

Fig. 6 shows the performance of extracted inherent features

for SAE-SS and SAE-TF under $SNR = -15\text{dB}$, compared with the input signals of the first layer. Specifically, the first 10^4 samples denote “PU is absent” and the second 10^4 samples mean “PU is present”. The numbers of input data of the first layer for SAE-SS and SAE-TF are 288 and 576, respectively. For each method, the number of output signals of the second hidden layer is 50. According to Fig. 6(a) and Fig. 6(c), it is very difficult to differentiate between the “PU is absent” and “PU is present” based on the input signals only. However, they can be readily separated by the output signals of the second hidden layer as is clear from Fig. 6(b) and Fig. 6(d), because the SAE-SS and SAE-TF can extract more inherent features included in signals.

A. Sensing Performance Comparison between proposed methods and Traditional OFDM Spectrum Sensing Methods

In this subsection, we compare the values of PM under different conditions for five sensing methods: the proposed SAE-SS, SAE-TF, ED [7], PT-based spectrum sensing methods [11] and CP-based [14], .

Fig. 7 compares the values of PM of different sensing methods under the perfect condition, respectively. The “perfect condition” means that the SU has enough prior knowledge of PU signals, and there is no effects of noise uncertainty, timing delay or carrier frequency offset. According to this figure, the values of PM of SAE-SS and SAE-TF are much smaller than the other three sensing methods. For instance, when $SNR = -20\text{dB}$, the PM of SAE-SS and SAE-TF are only 0.4992 and 0.2788, respectively. By contrast, the figures for ED, CP and PT sensing methods are 0.9225, 0.9114 and 0.9128, respectively. Moreover, with the increase of SNR, the PM of SAE-SS and SAE-TF obtain greater declines than other three sensing methods.

Fig. 8 shows the impact of noise uncertainty on five sensing methods with $SNR = -10\text{dB}$. According to this figure, it is clear that the proposed SAE-SS and SAE-TF are much robust to the noise uncertainty than other three sensing methods. For instance, when noise uncertainty increases from 0.5dB to 1dB, PM of SAE-SS and SAE-TF only increase from 0.0155 to 0.0190 and from 0.0096 to 0.0108, respectively. On the contrary, the PM of CP-based, PT-based and ED sensing methods increase from 0.2549 to 0.2991, from 0.1580 to 0.1899 and from 0.4899 to 0.5593, respectively.

Fig. 9 compares the effect of timing delay on sensing performance among different sensing methods. Since ED is not affected by timing delay, we only present the sensing performance of SAE-SS, SAE-TF, PT-based, and CP-based sensing methods. The timing delay, δ , is selected as 1-symbol and 5-symbol, respectively. It can be seen that with the comparison of PT-based and CP-based sensing methods, SAE-SS and SAE-TF are more robust to the timing delay. Moreover, the PM of SAE-TF is still the smallest of these four sensing methods even it suffers the timing delay. For instance, when $\delta = 5$ symbol and $SNR = -12\text{dB}$, the PM of SAE-SS and SAE-TF are 0.0679 and 0.0418, respectively. However, the PM of PT-based and CP-based are 0.5520 and 0.8756, respectively.

Fig. 10 shows the impact of CFO on four different sensing methods. The normalized CFO in this figure is set to 0.5 and

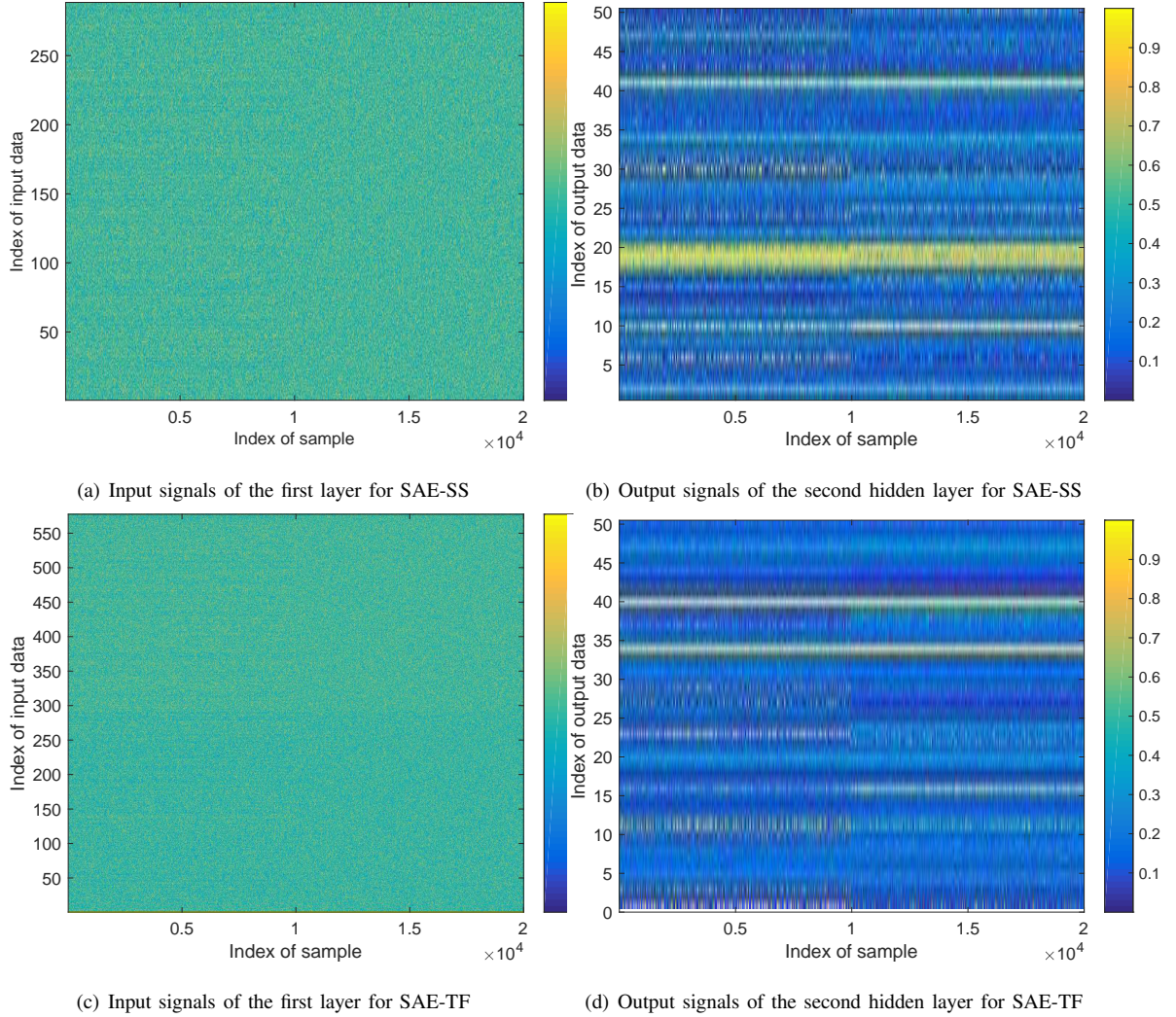


Fig. 6. The performance of extracting inherent features for SAE-SS and SAE-TF under SNR=-15dB

1. The sensing results of ED are not presented in this figure, because it is not affected by CFO. It is obvious that the proposed SAE-SS and SAE-TF outperform the CP-based and PT-based sensing methods regarding the robustness to CFO. The proposed SAE-SS and SAE-TF are capable of achieving much higher PM than the other two sensing methods. Moreover, the PM of SAE-SS and SAE-TF decrease slightly when the normalized CFO grows from 0.5 to 1. However, PM of the PT-based and CP-based methods decrease significantly. For example, when $f_q = 1$ and SNR = -10, PM of SAE-SS and SAE-TF are 0.0195 and 0.0130, respectively. However, those of PT-based and CP-based are 0.4810 and 0.5829, respectively.

B. Sensing Performance analysis of SAE-SS and SAE-TF under different conditions

In this subsection, we further analyze the sensing performance of the proposed SAE-SS and SAE-TF under different conditions.

Fig. 11 shows the impact of the number of hidden layers on SAE-SS and SAE-TF. The number of hidden layers is selected as $L = 1, 2, 3$, respectively. According to this figure, the values

of PM for these two sensing methods are getting better with the increase of L . For example, when L increases from 1 to 3, SNR = -20dB, the PM of SAE-SS and SAE-TF decrease from 0.5871 to 0.4731 and from 0.3260 to 0.2213, respectively. However, the complexities of these two methods would also increase, thus specific L should be selected based on different circumstances.

Fig. 12 compares the values of PM for SAE-SS and SAE-TF with different number of hidden units under SNR = -18dB. Regarding this figure, both of these two methods can achieve smaller values of PM with the increase in the number of hidden units. Moreover, the value of PM for SAE-TF get a bigger decrease than that of SAE-SS when increasing the number of hidden units.

Fig. 13 shows the sensing performance of SAE-SS and SAE-TF with different M . According to this figure, it is obvious that the sensing performance of these two sensing methods are affected by the factor M . When M changes from 1 to 3, SNR = -10dB, the PM of SAE-SS declines from 0.0453 to 0.0051, and the PM of SAE-TF decreases from 0.0231 to 0.0011. Notably, the complexity also increases with the growth of M , which will be demonstrated in Table I.

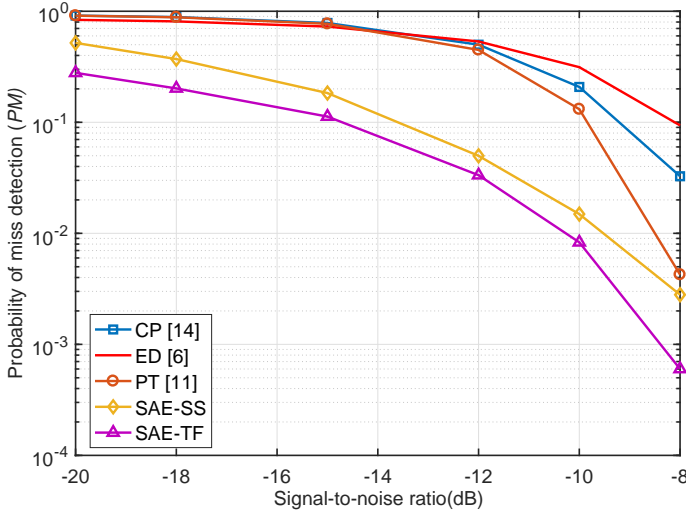


Fig. 7. Probability of miss detection among different spectrum sensing methods under perfect conditions

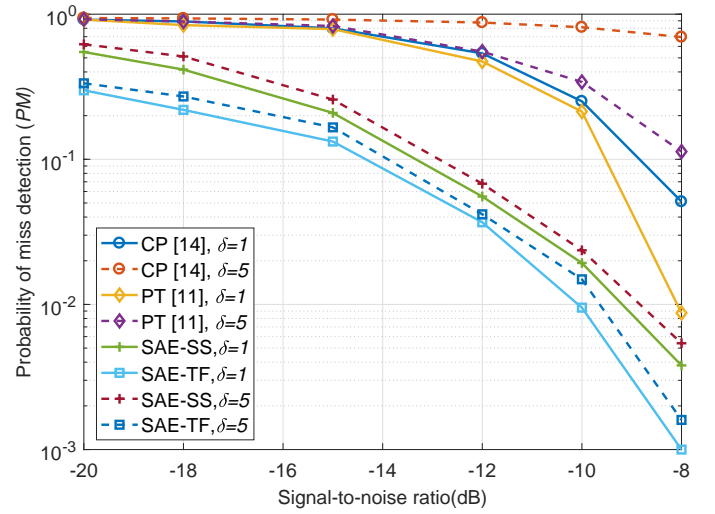


Fig. 9. Probability of miss detection among different spectrum sensing methods with timing delay

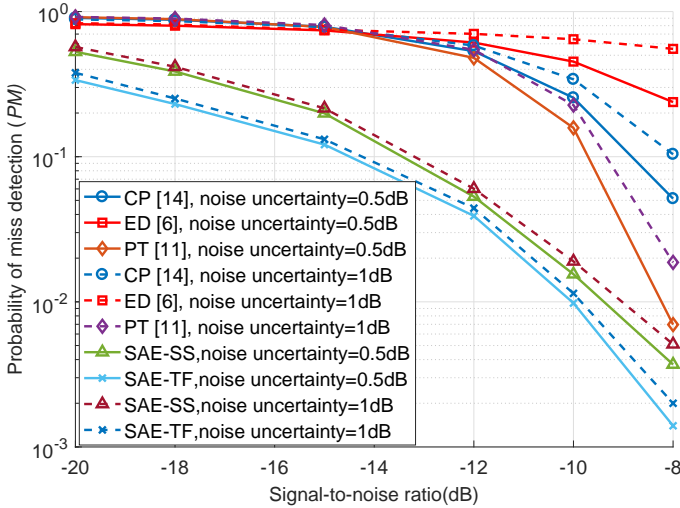


Fig. 8. Probability of miss detection among different spectrum sensing methods with noise uncertainty

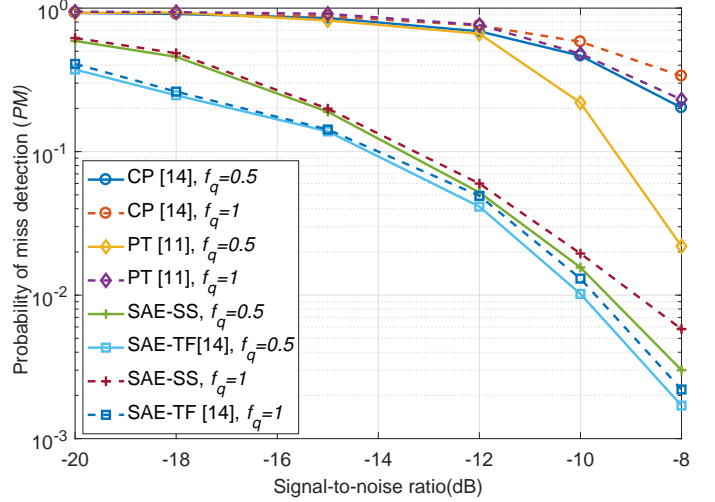


Fig. 10. Probability of miss detection among different spectrum sensing methods with timing delay

Table I shows the offline training time of SAE-SS and SAE-TF with a different number of OFDM blocks. We utilize a 6-Core 3.6GHz PC with Nvidia P5000 graphic card (16GB memory) to train the SAE-SS and SAE-TF. The training data set contains 10^6 samples. The number of interaction is 20000. Based on this table, the offline training time of SAE-TF is bigger than that of SAE-SS. Moreover, with the increase

TABLE I
OFFLINE TRAINING TIME FOR SAE-SS AND SAE-TF

Methods	M		
	$M = 1$	$M = 2$	$M = 3$
SAE-SS	104.68mins	159.32mins	254.15mins
SAE-TF	122.47mins	321.92mins	451.24mins

of M , the offline training time of SAE-TF is increasingly longer than SAE-SS. Since SAE-TF can achieve better sensing performance than SAE-SS, users can choose specific methods depending on different circumstances.

VI. CONCLUSION

In this paper, we proposed a Stacked Autoencoder Based Spectrum Sensing Method (SAE-SS) and a Stacked Autoencoder Based Spectrum Sensing Method with time-frequency domain signals (SAE-TF) to detect the activity states of PUs. SAE-SS and SAE-TF are more robust to timing delay, CFO, and noise uncertainty, compared with the conventional OFDM sensing methods. Moreover, they are able to detect PU's signals based on the received signals only, without any requirement of prior knowledge of PU's signals. SAE-SS can complete the sensing mask using the original received signals

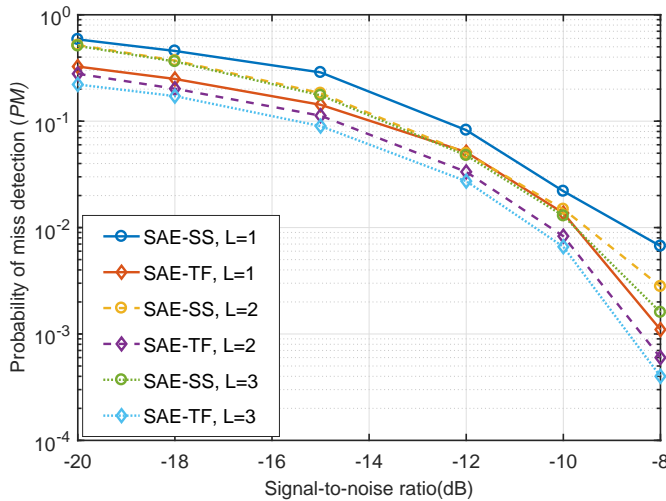


Fig. 11. Probability of miss detection of SAE-SS and SAE-TF with different number of hidden layers

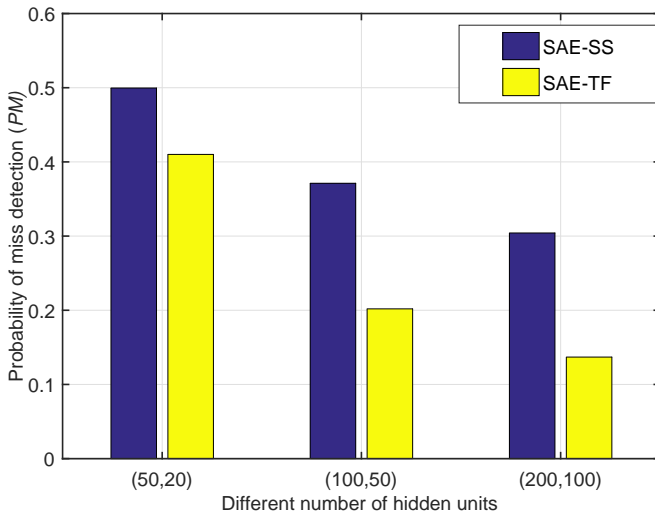


Fig. 12. Probability of miss detection of SAE-SS and SAE-TF with different number of hidden units

only without any additional feature extraction processing. SAE-TF can achieve a better sensing accuracy than SAE-SS, especially under low SNR conditions, while it has a higher complexity. Extensive simulation results demonstrate that SAE-SS and SAE-TF are capable of achieving more better sensing performance than traditional OFDM sensing methods with poor conditions.

REFERENCES

- [1] W. y. Lee and I. F. Akyildiz, "Optimal spectrum sensing framework for cognitive radio networks," *IEEE Transactions on Wireless Communications*, vol. 7, no. 10, pp. 3845–3857, October 2008.
- [2] T. Yucek and H. Arslan, "A survey of spectrum sensing algorithms for cognitive radio applications," *IEEE Communications Surveys Tutorials*, vol. 11, no. 1, pp. 116–130, First 2009.
- [3] H. Tang, "Some physical layer issues of wide-band cognitive radio systems," in *First IEEE International Symposium on New Frontiers in*

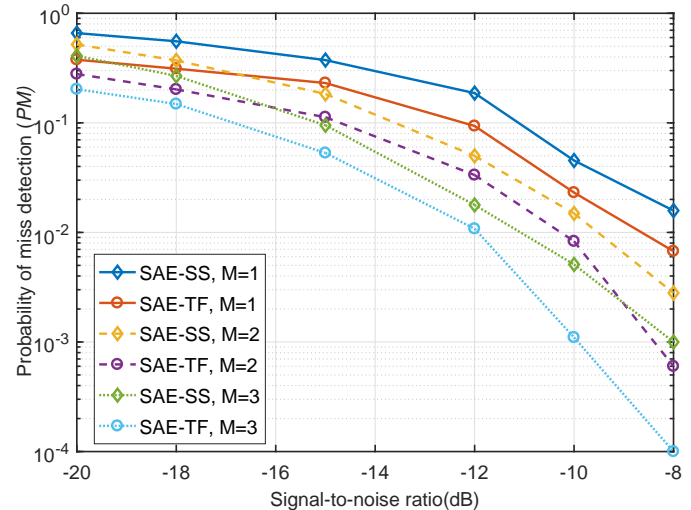


Fig. 13. Probability of miss detection of SAE-SS and SAE-TF with different M

Dynamic Spectrum Access Networks, 2005. DySPAN 2005., Nov 2005, pp. 151–159.

- [4] J. Tong, M. Jin, Q. Guo, and Y. Li, "Cooperative spectrum sensing: A blind and soft fusion detector," *IEEE Transactions on Wireless Communications*, vol. 17, no. 4, pp. 2726–2737, April 2018.
- [5] K. B. Letaief and W. Zhang, "Cooperative communications for cognitive radio networks," *Proceedings of the IEEE*, vol. 97, no. 5, pp. 878–893, May 2009.
- [6] W. L. Chin, C. W. Kao, and Y. Qian, "Spectrum sensing of OFDM signals over multipath fading channels and practical considerations for cognitive radios," *IEEE Sensors Journal*, vol. 16, no. 8, pp. 2349–2360, April 2016.
- [7] T. Riihonen and R. Wichman, "Energy detection in full-duplex cognitive radios under residual self-interference," in *2014 9th International Conference on Cognitive Radio Oriented Wireless Networks and Communications (CROWNCOM)*, June 2014, pp. 57–60.
- [8] R. Tandra and A. Sahai, "SNR walls for signal detection," *IEEE Journal of Selected Topics in Signal Processing*, vol. 2, no. 1, pp. 4–17, Feb 2008.
- [9] S. Bokharaiee, H. H. Nguyen, and E. Shwedyk, "Blind spectrum sensing for OFDM-based cognitive radio systems," *IEEE Transactions on Vehicular Technology*, vol. 60, no. 3, pp. 858–871, March 2011.
- [10] A. F. Eduardo and R. G. G. Caballero, "Experimental evaluation of performance for spectrum sensing: Matched filter vs energy detector," in *IEEE Colombian Conference on Communication and Computing (IEEE COLCOM 2015)*, May 2015, pp. 1–6.
- [11] Z. Chen, T. Luan, and X. D. Zhang, "Sensing orthogonal frequency division multiplexing systems for cognitive radio with cyclic prefix and pilot tones," *IET Communications*, vol. 6, no. 1, pp. 97–106, January 2012.
- [12] H. s. Chen, W. Gao, and D. G. Daut, "Spectrum sensing for OFDM systems employing pilot tones," *IEEE Transactions on Wireless Communications*, vol. 8, no. 12, pp. 5862–5870, December 2009.
- [13] Z. Lu, Y. Ma, P. Cheraghi, and R. Tafazolli, "Novel pilot-assisted spectrum sensing for OFDM systems by exploiting statistical difference between subcarriers," *IEEE Transactions on Communications*, vol. 61, no. 4, pp. 1264–1276, April 2013.
- [14] E. Axell and E. G. Larsson, "Optimal and sub-optimal spectrum sensing of OFDM signals in known and unknown noise variance," *IEEE Journal on Selected Areas in Communications*, vol. 29, no. 2, pp. 290–304, February 2011.
- [15] S. Chaudhari, V. Koivunen, and H. V. Poor, "Autocorrelation-based decentralized sequential detection of OFDM signals in cognitive radios," *IEEE Transactions on Signal Processing*, vol. 57, no. 7, pp. 2690–2700, July 2009.
- [16] M. Kim, K. Po, and J. i. Takada, "Performance enhancement of cyclostationarity detector by utilizing multiple cyclic frequencies of OFDM signals," in *2010 IEEE Symposium on New Frontiers in Dynamic Spectrum (DySPAN)*, April 2010, pp. 1–8.

- [17] W. Xu, W. Xiang, M. El-kashlan, and H. Mehrpouyan, "Spectrum sensing of OFDM signals in the presence of carrier frequency offset," *IEEE Transactions on Vehicular Technology*, vol. 65, no. 8, pp. 6798–6803, Aug 2016.
- [18] Z. Lei and F. P. S. Chin, "Sensing OFDM systems under frequency-selective fading channels," *IEEE Transactions on Vehicular Technology*, vol. 59, no. 4, pp. 1960–1968, May 2010.
- [19] M. Jin, Q. Guo, J. Xi, Y. Li, and Y. Li, "On spectrum sensing of OFDM signals at low SNR: New detectors and asymptotic performance," *IEEE Transactions on Signal Processing*, vol. 65, no. 12, pp. 3218–3233, June 2017.
- [20] S. Zhang, Y. Sui, S. Zhao, and L. Zhang, "Graph-regularized structured support vector machine for object tracking," *IEEE Transactions on Circuits and Systems for Video Technology*, vol. 27, no. 6, pp. 1249–1262, June 2017.
- [21] S. Zhang, X. Yu, Y. Sui, S. Zhao, and L. Zhang, "Object tracking with multi-view support vector machines," *IEEE Transactions on Multimedia*, vol. 17, no. 3, pp. 265–278, March 2015.
- [22] L. Deng and X. Li, "Machine learning paradigms for speech recognition: An overview," *IEEE Transactions on Audio, Speech, and Language Processing*, vol. 21, no. 5, pp. 1060–1089, May 2013.
- [23] S. Zhang, S. Zhang, T. Huang, and W. Gao, "Speech emotion recognition using deep convolutional neural network and discriminant temporal pyramid matching," *IEEE Transactions on Multimedia*, vol. 20, no. 6, pp. 1576–1590, June 2018.
- [24] H. Ye, G. Y. Li, and B. H. Juang, "Power of deep learning for channel estimation and signal detection in ofdm systems," *IEEE Wireless Communications Letters*, vol. 7, no. 1, pp. 114–117, Feb 2018.
- [25] L. He, G. Wang, and Z. Hu, "Learning depth from single images with deep neural network embedding focal length," *IEEE Transactions on Image Processing*, vol. 27, no. 9, pp. 4676–4689, Sept 2018.
- [26] G. Tello, O. Y. Al-Jarrah, P. D. Yoo, Y. Al-Hammadi, S. Muhaidat, and U. Lee, "Deep-structured machine learning model for the recognition of mixed-defect patterns in semiconductor fabrication processes," *IEEE Transactions on Semiconductor Manufacturing*, vol. 31, no. 2, pp. 315–322, May 2018.
- [27] H. C. Shin, M. R. Orton, D. J. Collins, S. J. Doran, and M. O. Leach, "Stacked autoencoders for unsupervised feature learning and multiple organ detection in a pilot study using 4d patient data," *IEEE Transactions on Pattern Analysis and Machine Intelligence*, vol. 35, no. 8, pp. 1930–1943, Aug 2013.
- [28] Y. Bengio, "Learning deep architectures for ai," *Foundations and Trends in Machine Learning*, vol. 2, no. 1, pp. 1–127, 2009. [Online]. Available: <http://dx.doi.org/10.1561/22000000006>
- [29] J. Lu, V. E. Liong, G. Wang, and P. Moulin, "Joint feature learning for face recognition," *IEEE Transactions on Information Forensics and Security*, vol. 10, no. 7, pp. 1371–1383, July 2015.
- [30] M. R. Vyas, D. K. Patel, and M. Lopez-Benitez, "Artificial neural network based hybrid spectrum sensing scheme for cognitive radio," in *2017 IEEE 28th Annual International Symposium on Personal, Indoor, and Mobile Radio Communications (PIMRC)*, Oct 2017, pp. 1–7.
- [31] Y. J. Tang, Q. Y. Zhang, and W. Lin, "Artificial neural network based spectrum sensing method for cognitive radio," in *2010 6th International Conference on Wireless Communications Networking and Mobile Computing (WiCOM)*, Sept 2010, pp. 1–4.
- [32] D. Han, G. C. Sobabe, C. Zhang, X. Bai, Z. Wang, S. Liu, and B. Guo, "Spectrum sensing for cognitive radio based on convolution neural network," in *2017 10th International Congress on Image and Signal Processing, BioMedical Engineering and Informatics (CISP-BMEI)*, Oct 2017, pp. 1–6.
- [33] O. Sigaud and A. Droniou, "Towards deep developmental learning," *IEEE Transactions on Cognitive and Developmental Systems*, vol. 8, no. 2, pp. 99–114, June 2016.
- [34] H. F. Yang, T. S. Dillon, and Y. P. P. Chen, "Optimized structure of the traffic flow forecasting model with a deep learning approach," *IEEE Transactions on Neural Networks and Learning Systems*, vol. 28, no. 10, pp. 2371–2381, Oct 2017.
- [35] J. Schmidhuber, "Deep learning in neural networks: An overview," *Neural Networks*, vol. 61, no. Supplement C, pp. 85 – 117, 2015. [Online]. Available: <http://www.sciencedirect.com/science/article/pii/S0893608014002135>
- [36] Y. Cao, C. Shen, and H. T. Shen, "Exploiting depth from single monocular images for object detection and semantic segmentation," *IEEE Transactions on Image Processing*, vol. 26, no. 2, pp. 836–846, Feb 2017.
- [37] Y. Bengio, P. Lamblin, D. Popovici, and H. Larochelle, "Greedy layer-wise training of deep networks," in *Advances in neural information processing systems*, 2007, pp. 153–160.
- [38] B. Matter, *Iterative Methods for Optimization*, pp. 161–180. [Online]. Available: <http://epubs.siam.org/doi/abs/10.1137/1.9781611970920.bm>